set (Fig. 3B), and we extracted a Bell state fidelity of 0.72, which demonstrates the production of an entangled state. For $\tau = \tau_{ent} = \frac{\pi}{(2J_{12})} = 160$ ns (Fig. 3C), we see a similar state to $\tau = 140$ ns, but with less weight in the single-qubit components of the Pauli set. This state corresponds to the intended CPhase of π, although the fidelity is slightly lower than at $\tau = 140$ ns due to additional decoherence. Finally, at $\tau = \pi/J_{12} = 320$ ns (Fig. 3D), where we expect the state to be unentangled, we again see large weight in the $\langle YI \rangle$, $\langle IY \rangle$, and $\langle YY \rangle$ components of the Pauli set, although the bars are shorter than the Pauli set for $\tau = 40$ ns because of dephasing of the qubits. We plotted the entire Pauli set as a function of time (Fig. 3E), which clearly shows the predicted oscillation (Eq. 2) between $\langle YI \rangle$,$\langle IY \rangle$ and $\langle XZ \rangle$,$\langle ZX \rangle$, with decays due to decoherence.

The two-qubit gate that we have demonstrated is an important step toward establishing a scalable architecture for quantum information processing in S-T_0 qubits. Although a Bell state fidelity of 0.72 is not as high as what has been reported in other solid state implementations of qubits (*21*, *27*), there are easily implemented improvements to this two-qubit gate. State fidelity is lost to dephasing from electrical noise, and decreasing the ratio τ_{ent}/T_2^{echo}, where T_2^{echo} is the single-qubit coherence time with an echo pulse, is therefore paramount to generating high-fidelity Bell states. Large improvements can be made by introducing an electrostatic coupler between the two qubits (*28*) to increase the two-qubit coupling (J_{12}) and reduce τ_{ent}. We estimate that in the absence of other losses, if an electrostatic coupler were used, a Bell state with fidelity exceeding 90% could be produced. Other improvements can be made by studying the origins and properties of the charge noise that dephases the qubit and mitigating its adverse effects in order to increase T_2^{echo}. This would allow future tests of complex quantum operations, including quantum algorithms and quantum error correction. Finally, the addition of electrostatic couplers would allow the qubits to be spacially separated and is a path toward implementing surface codes for quantum computation.

References and Notes

1. D. Loss, D. P. DiVincenzo, *Phys. Rev. A* **57**, 120 (1998).
2. F. H. L. Koppens *et al.*, *Nature* **442**, 766 (2006).
3. M. Pioro-Ladriere *et al.*, *Nat. Phys.* **4**, 776 (2008).
4. K. C. Nowack, F. H. L. Koppens, Y. V. Nazarov, L. M. K. Vandersypen, *Science* **318**, 1430 (2007).
5. M. Pioro-Ladriere, Y. Tokura, T. Kubo, S. Tarucha, *Appl. Phys. Lett.* **90**, 024105 (2007).
6. H. O. H. Churchill *et al.*, *Phys. Rev. Lett.* **102**, 166802 (2009).
7. S. Nadj-Perge, S. M. Frolov, E. P. Bakkers, L. P. Kouwenhoven, *Nature* **468**, 1084 (2010).
8. J. Levy, *Phys. Rev. Lett.* **89**, 147902 (2002).
9. J. R. Petta *et al.*, *Science* **309**, 2180 (2005).
10. J. M. Taylor *et al.*, *Phys. Rev. B* **76**, 035315 (2007).
11. S. Foletti, H. Bluhm, D. Mahalu, V. Umansky, A. Yacoby, *Nat. Phys.* **5**, 903 (2009).
12. H. Bluhm, S. Foletti, D. Mahalu, V. Umansky, A. Yacoby, *Phys. Rev. Lett.* **105**, 216803 (2010).
13. D. J. Reilly, C. M. Marcus, M. P. Hanson, A. C. Gossard, *Appl. Phys. Lett.* **91**, 162101 (2007).
14. C. Barthel, D. J. Reilly, C. M. Marcus, M. P. Hanson, A. C. Gossard, *Phys. Rev. Lett.* **103**, 160503 (2009).
15. M. A. Nielsen, I. L. Chuang, *Quantum Computation and Quantum Information* (Cambridge Univ. Press, Cambridge, 2000).
16. J. M. Taylor *et al.*, *Nat. Phys.* **1**, 177 (2005).
17. L. Viola, E. Knill, S. Lloyd, *Phys. Rev. Lett.* **82**, 2417 (1999).
18. D. Leibfried *et al.*, *Nature* **422**, 412 (2003).
19. E. L. Hahn, *Phys. Rev.* **80**, 580 (1950).
20. F. V. Daniel, *Phys. Rev. A* **64**, 052312 (2001).
21. J. M. Chow *et al.*, *Phys. Rev. A* **81**, 062325 (2010).
22. S. Hill, W. Wootters, *Phys. Rev. Lett.* **78**, 5022 (1997).
23. C. A. Sackett *et al.*, *Nature* **404**, 256 (2000).
24. C. H. Bennett *et al.*, *Phys. Rev. Lett.* **76**, 722 (1996).
25. T. Yu, J. H. Eberly, *Opt. Commun.* **264**, 393 (2006).
26. L. Cywinski, R. M. Lutchyn, C. P. Nave, S. Das Sarma, *Phys. Rev. B* **77**, 174509 (2008).
27. M. Ansmann *et al.*, *Nature* **461**, 504 (2009).
28. L. Trifunovic *et al.*, *Phys. Rev. X* **2**, 011006 (2012).

Acknowledgments: This work is supported through the U.S. Army Research Office (ARO) Precision Quantum Control and Error-Suppressing Quantum Firmware for Robust Quantum Computing and the Intelligence Advanced Research Projects Activity (IARPA) Multi-Qubit Coherent Operations (MQCO) Program. This work was partially supported by the ARO under contract W911NF-11-1-0068. This work was performed in part at the Center for Nanoscale Systems (CNS), a member of the National Nanotechnology Infrastructure Network (NNIN), which is supported by the National Science Foundation under NSF award ECS-0335765. CNS is part of Harvard University. V.U. prepared the crystal; M.D.S. fabricated the sample; and M.D.S., O.E.D., H.B., S.P.H., and A.Y. carried out the experiment, analyzed the data, and wrote the paper. The authors declare no competing financial interests.

Supplementary Materials

www.sciencemag.org/cgi/content/full/336/6078/202/DC1
Materials and Methods
Figs. S1 to S5
References

9 December 2011; accepted 7 March 2012
10.1126/science.1217692

Topological Transitions in Metamaterials

Harish N. S. Krishnamoorthy,[1,2]* Zubin Jacob,[3]* Evgenii Narimanov,[4] Ilona Kretzschmar,[5] Vinod M. Menon[1,2]†

Light-matter interactions can be controlled by manipulating the photonic environment. We uncovered an optical topological transition in strongly anisotropic metamaterials that results in a dramatic increase in the photon density of states—an effect that can be used to engineer this interaction. We describe a transition in the topology of the iso-frequency surface from a closed ellipsoid to an open hyperboloid by use of artificially nanostructured metamaterials. We show that this topological transition manifests itself in increased rates of spontaneous emission of emitters positioned near the metamaterial. Altering the topology of the iso-frequency surface by using metamaterials provides a fundamentally new route to manipulating light-matter interactions.

Metamaterials are artificial media in which the subwavelength features of the designed unit cells and coupling between them governs the macroscopic electromagnetic properties (*1*). This control over material parameters has led to new applications (*2*–*4*) and also the ability to mimic and study physical processes, which is difficult by other methods (*5*–*7*). One specific design freedom afforded by metamaterials is the control over the iso-frequency surface, the surface of allowed wavevectors at constant frequency (*8*, *9*). The topology of this surface governs wave dynamics inside a medium.

The ideas of mathematical topology play an important role in many aspects of modern physics, from phase transitions to field theory to nonlinear dynamics (*10*, *11*). An important example of this is the Lifshitz transition (*12*), in which the transformation of the Fermi surface of a metal from a closed to an open geometry (because of, for example, external pressure) leads to a dramatic effect on the electron magneto-transport (*13*). In optics, the role of the Fermi surface is played by the optical iso-frequency surface $\omega(\vec{k}) = const$, which can be engineered by tailoring the dielectric tensor, $\overleftrightarrow{\varepsilon}(\vec{r})$. We use this to demonstrate the optical equivalent of the "Lifshitz transition"—the optical topological transition (OTT) in which the very nature of the electromagnetic radiation in the metamaterial undergoes a drastic change. Effects on the kinetic and thermodynamic properties, such as the dynamics of propagating waves supported by the system and the electromagnetic energy density, respectively, are modified at the transition point and can be probed by following the light-metamaterial interaction using a quantum emitter.

We considered a metamaterial structure that has a uniaxial form of the dielectric tensor $\overleftrightarrow{\varepsilon}(\vec{r}) = diag(\varepsilon_{xx}, \varepsilon_{yy}, \varepsilon_{zz})$, where $\varepsilon_{xx} = \varepsilon_{yy} = \varepsilon_{\parallel}$ and $\varepsilon_{zz} = \varepsilon_{\perp}$. The iso-frequency surface for the extraordinary (TM-polarized) waves propagating in such a strongly anisotropic metamaterial is given by

$$\frac{k_x^2 + k_y^2}{\varepsilon_{\perp}} + \frac{k_z^2}{\varepsilon_{\parallel}} = \frac{\omega^2}{c^2} \qquad (1)$$

Closed iso-frequency surfaces differing from a simple sphere (such as an ellipsoid) can occur in these metamaterials when $\varepsilon_{\parallel}, \varepsilon_{\perp} > 0$ and

[1]Department of Physics, Queens College, City University of New York (CUNY) and Center for Photonic and Multiscale Nanomaterials, Flushing, NY 11367, USA. [2]Department of Physics, Graduate Center, CUNY, New York, NY 10016, USA. [3]Department of Electrical and Computer Engineering, University of Alberta, Edmonton T6G 2V4, Canada. [4]Birck Nanotechnology Center, School of Electrical and Computer Engineering, Purdue University, West Lafayette, IN 47907, USA. [5]Department of Chemical Engineering, City College, CUNY, New York, NY 10031, USA.

*These authors contributed equally to this work.
†To whom correspondence should be addressed. E-mail: vmenon@qc.cuny.edu

$\varepsilon_{\parallel} \neq \varepsilon_{\perp}$. On the other hand, an extreme modification of the iso-frequency surface into a hyperboloid occurs when the dielectric constants show opposite sign ($\varepsilon_{\parallel} < 0$ and $\varepsilon_{\perp} > 0$). We can design a metamaterial so that the dispersion of the dielectric constants leads to an OTT in the iso-frequency surface from an ellipsoid to a hyperboloid.

The photonic density of states (PDOS) in the metamaterial is related to the volume enclosed by the corresponding iso-frequency surface (*14*). Therefore, the topological transition from the closed (ellipsoid) iso-frequency surface for $\varepsilon_{\parallel} > 0$ to an open (hyperboloid) iso-frequency surface for $\varepsilon_{\parallel} < 0$ (Fig. 1) results in a nonintegrable singularity accompanied by a change in the density of states from a finite to an infinite value (in lossless effective medium limit). This optical analog of the Lifshitz transition in metamaterials is characterized by the appearance of additional electromagnetic states in the hyperbolic regime, which have wave vectors much larger than those allowed in vacuum. Light-matter interaction is enhanced because of the presence of these additional electromagnetic states, resulting in a strong effect on related quantum-optical phenomena, such as spontaneous emission.

The decay rate near a half space of a metamaterial for a dipole-like emitter is given by (*15*–*20*)

$$\Gamma = \Gamma_{vac} + \Gamma_{plasmon} + \Gamma_{high-k} \qquad (2)$$

where Γ_{vac} and $\Gamma_{plasmon}$ are the decay rates due to propagating waves in vacuum and the surface plasmon polariton (SPP) modes supported by the metamaterial, respectively, and Γ_{high-k} is the decay rate enhancement due to the high–wave vector states, which appear only beyond the OTT. In the near field of the metamaterial, when $d << \lambda$ the decay rate is dominated by the contribution from the high–wave vector states (*21*):

$$\Gamma_{high-k} \approx \frac{\mu_{\perp}^2 Im(r_p)}{8\hbar d^3} \qquad (3)$$

where $\mu_{\perp}$ is the dipole moment of the perpendicularly oriented dipole, r_p is the plane wave reflection coefficient of p-polarized light (*21*), and d is the distance of the dipole from the interface. In a hyperbolic metamaterial half space where $real(\varepsilon_{\parallel}) < 0$

$$Im(r_p) = \frac{2\sqrt{|\varepsilon_{\parallel}|\varepsilon_{\perp}}}{1 + |\varepsilon_{\parallel}|\varepsilon_{\perp}} \qquad (4)$$

and for $[real(\varepsilon_{\parallel}) > 0]$, we have an elliptical dispersion with $Im(r_p) = 0$ (assuming no losses). We thus introduce the topological transition parameter $\alpha = Im(r_p)$, which is proportional to the local density of electromagnetic modes and characterizes the emergence of high-k metamaterial states. The effect of dispersive and lossy effective medium dielectric constants on the topological transition parameter (proportional to the spontaneous emission rate) is shown in Fig. 2A. Although the losses reduce the sharp transition to a smooth crossover, the change in the iso-frequency surface topology still leads to an enhanced spontaneous emission rate.

Metamaterials with opposite signs of the dielectric constants can be realized by using metal-dielectric composites (*22*). We considered such a composite consisting of alternating layers of silver (9 nm) and titanium dioxide (TiO_2) (22 nm) corresponding to a 29% fill fraction of silver. Using the semiclassical theory of spontaneous

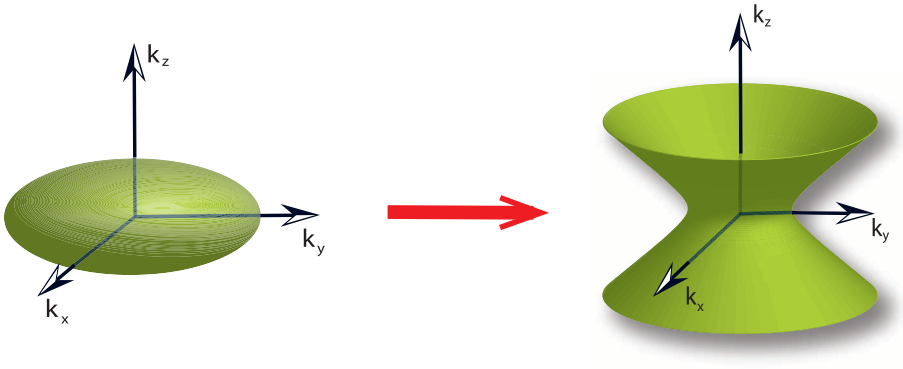

Fig. 1. OTT: The optical iso-frequency curve changes from a closed surface such as an ellipsoid to an open hyperboloid.

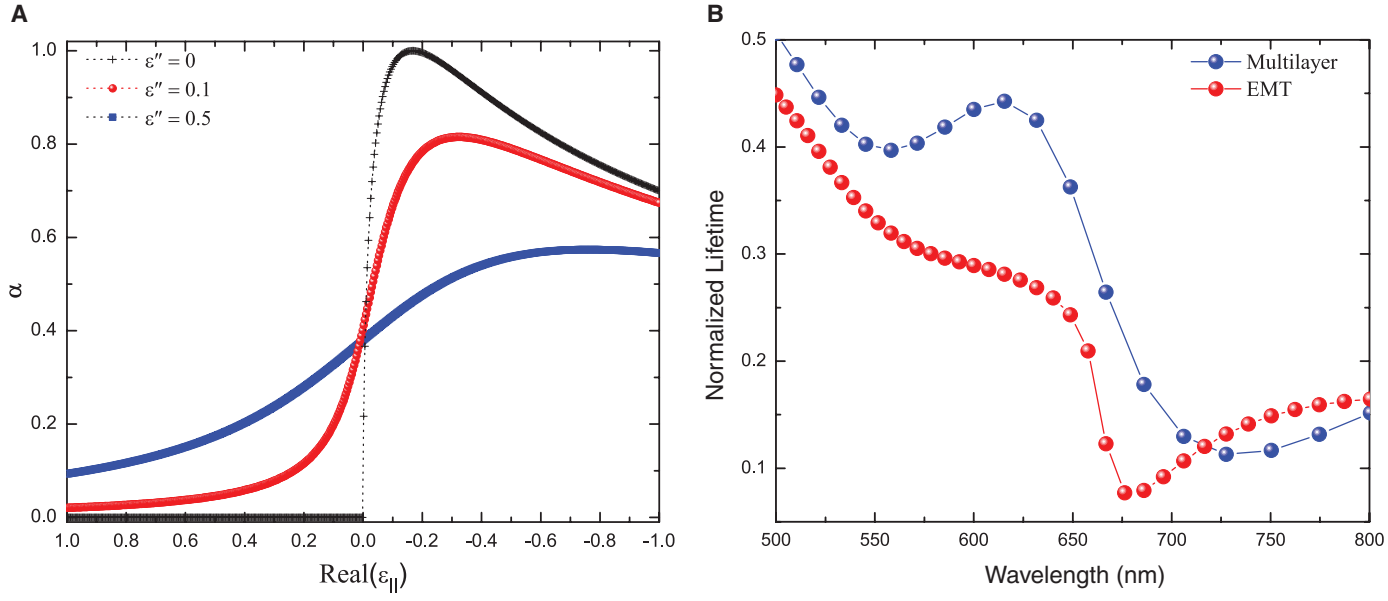

Fig. 2. (**A**) Topological transition parameter (proportional to the local density of states) near the topological transition wavelength as a function of the real part of $\varepsilon_{\parallel}$. The sharp transition becomes a smooth crossover as losses are increased. (**B**) Lifetime of emitters placed on a practical realization of the metamaterial consisting of alternating layers of metal (silver, 9 nm) and dielectric (TiO_2, 22 nm) corresponding to the 29% fill fraction sample. A sharp reduction in the spontaneous emission lifetime is observed around the transition wavelength.

emission (*23*), we calculated the lifetime for quantum dots (QDs) placed in the near field of this metamaterial. Our simulation takes into account nonidealities arising because of realistic losses, dispersion, finite thickness of layers, sample size, and the substrate. Even in a practical structure (Fig. 2B), a clear modification in lifetime of the emitter is expected as the system transitions from elliptical to the hyperbolic dispersion regime over the spectral range of interest. The transition occurs because of the particular dispersion of coupled plasmons, which contribute to lifetime decrease only on the hyperbolic side of the transition (*21*). Simulations carried out through effective medium theory (EMT) show good agreement with the prediction of numerical simulations (Fig. 2B).

To experimentally observe the signature of the predicted OTT manifested through enhancement in spontaneous emission rate, we investigated a metamaterial structure similar to that discussed above with multiple QD emitters positioned on its top surface (Fig. 3A) (*21*). The dielectric constants of the constituent thin films were extracted by using ellipsometry, and the effective medium parameters are shown in Fig. 3B. This structure is designed to have $\varepsilon_{\parallel} \approx 0$ around 621 nm, which corresponds to the emission maximum of the CdSe/ZnS colloidal QDs used in the experiment. The photoluminescence (PL) from the QDs has a full width at half maximum (FWHM) of ~40 nm, which allows investigation of the phase space of both elliptical and hyperbolic dispersion regimes by use of the same sample. In order to isolate the effects of the nonradiative decay and SPP-based enhancement in the radiative rate due to the metal, we also measured the spontaneous emission rates of QDs on a control sample that consisted of one unit cell of the metamaterial (*21*).

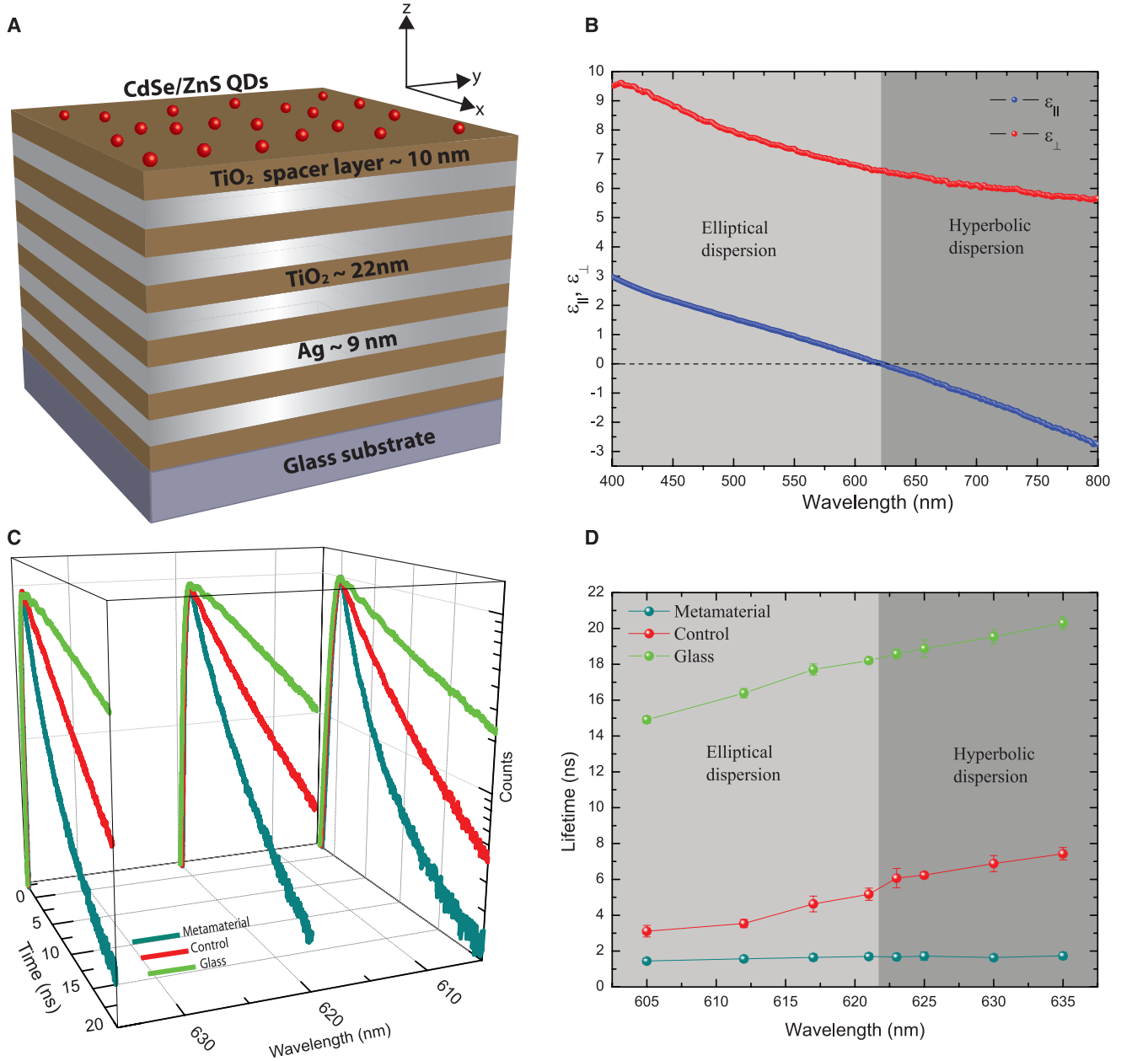

Fig. 3. (**A**) Schematic of the metamaterial structure. (**B**) Effective dielectric constants (real parts) of the structure determined with ellipsometry and effective medium theory. The transition from elliptical to hyperbolic dispersion occurs at 621 nm. (**C**) Time-resolved photoluminescence data from QDs deposited on the metamaterial, control sample, and glass substrate at 605, 621, and 635 nm. Clear reduction in lifetime is observed over 30-nm spectral bandwidth when the emitter is placed on the metamaterial. (**D**) Lifetime of the QDs as a function of wavelength on metamaterial, control sample, and glass substrate. QDs on the control sample and glass shows an increase in the lifetime with wavelength, whereas on the metamaterial, a slight decrease in lifetime is observed.

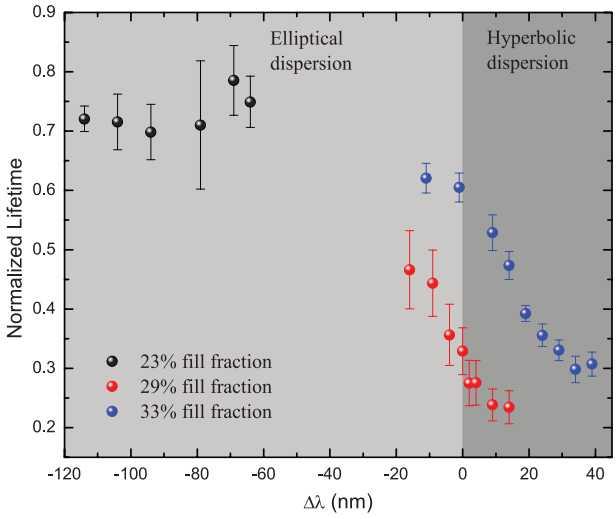

Fig. 4. The lifetime on the metamaterial structures normalized with respect to the control samples. The wavelength axis has been normalized with respect to the transition wavelength to compare the three samples. Here, positive and negative Δλ correspond to hyperbolic and elliptical dispersion regimes, respectively. The samples with fill fractions of 29 and 33% show the OTT manifested through sharp reduction in spontaneous emission lifetime when crossing over to the hyperbolic dispersion regime. On the contrary, the sample with 23% fill fraction, which lies in the elliptical dispersion regime, does not show such a reduction in lifetime. The experimentally observed transition is in good agreement with the theoretical prediction of Fig. 2B.

Time-resolved PL measurements were carried out on the metamaterial sample, the control sample, and the glass substrate (Fig. 3C) at the anticipated transition wavelength (621nm) and at spectral positions on either side (605 and 635 nm). The large change in the spontaneous emission lifetime of the QDs on the metamaterial compared with the glass substrate is due to the excitation of the high-k metamaterial states as well as the nonradiative contribution and the SPP modes of the metamaterial. When compared with the control sample, the metamaterial shows an enhancement in the spontaneous emission rate by a factor of ~3 at the transition wavelength and ~4.3 deeper in the hyperbolic regime (635 nm). These enhancements are attributed to the high-k metamaterial states. The overall reduction in the lifetime of the QDs when compared with those on a glass substrate is ~11.

The lifetime of the QDs increases as a function of wavelength on both the glass substrate and the control sample (Fig. 3D). This is due to the size distribution of QDs and the dependence of the oscillator strength on the energy (*24*–*26*). On the contrary, the metamaterial sample shows a decrease in the lifetime as a function of wavelength and the shortest lifetime owing to coupling to the high-k metamaterial states (Fig. 3D). The coupling of the emission from the QDs into the metamaterial states was also verified by using steady-state PL measurements (fig. S6) in which a reduction in the PL intensity emitted in the direction away from the metamaterial sample was observed (*21*, *27*).

To demonstrate the OTT, we studied the radiative lifetimes in three samples with differing volume ratio of metal to dielectric, which correspond to different transition wavelengths. We compared the lifetimes of the sample with 29% fill fraction of silver to one with 23% fill fraction, which lies deep in the elliptical phase, and to another sample that lies deeper in the hyperbolic phase, with fill fraction of 33% (*21*). To make any conclusions regarding the effect of the OTT on the radiative lifetimes from the measurement of the total decay rates, the contribution of the high-k metamaterial states has to be distinguished from nonradiative decay and the SPP-assisted decay of the unit cell. Because the spacer and first-layer environment of the QDs is the same in the control and the metamaterial sample, we expected similar quantum yield dependence on wavelength owing to near-field interaction of the QDs and the metallic structure. Thus, to account for purely the contribution from the high-k metamaterial states to the overall lifetime change, we normalized the QD lifetime on the metamaterials with that on the control samples (Fig. 4). The controls for the three samples are different and correspond to the unit cell of each metamaterial sample. To compare these three samples, which have OTTs at different wavelengths, we normalized the wavelength with respect to the transition wavelength, with positive and negative Δλ corresponding to the hyperbolic and elliptical dispersion regimes, respectively.

We clearly observed a sharp reduction in the normalized lifetime of the samples with 29 and 33% fill fractions that cross the transition wavelength, whereas the sample with 23% fill fraction, which lies in the elliptical regime, did not show this reduction. Whereas the combination of metal losses and finite thickness of layers leads to a smooth crossover, the signature of the transition is clear from the reduction in the normalized lifetime in the hyperbolic regime. The difference in the absolute value of the normalized lifetimes in the two samples that show the transitions is due to the differing fill fractions (29 versus 33%) and associated difference in the dielectric constants. Thus, the changes in the lifetime observed experimentally in these metamaterial structures can be attributed to the increase in the photonic density of states that manifests when the system goes through the topological transition in its isofrequency surface from an ellipsoid to a hyperboloid, which is in good agreement with the theoretical prediction of Fig. 2B.

We have established the occurrence of OTT in two metamaterial structures using spontaneous emission from a quantum emitter as the probe. Absence of OTT in a structure that lies solely in the elliptical dispersion phase has also been demonstrated. A host of interesting effects can transpire at the transition wavelength, such as the sudden appearance of resonance cones, which are characteristic of hyperbolic metamaterials (*28*), enhanced nonlinear effects, and abrupt changes in the electromagnetic energy density. We expect the OTT to be the basis for a number of applications of both fundamental and technological importance through use of metamaterial-based control of light-matter interaction.

References and Notes

1. V. M. Shalaev, *Nat. Photonics* **1**, 41 (2007).
2. J. B. Pendry, *Phys. Rev. Lett.* **85**, 3966 (2000).
3. J. B. Pendry, D. Schurig, D. R. Smith, *Science* **312**, 1780 (2006).
4. U. Leonhardt, *Science* **312**, 1777 (2006).
5. D. A. Genov, S. Zhang, X. Zhang, *Nat. Phys.* **5**, 687 (2009).
6. E. E. Narimanov, A. V. Kildishev, *Appl. Phys. Lett.* **95**, 041106 (2009).
7. I. I. Smolyaninov, E. E. Narimanov, *Phys. Rev. Lett.* **105**, 067402 (2010).
8. Z. Jacob, L. V. Alekseyev, E. Narimanov, *Opt. Express* **14**, 8247 (2006).
9. Z. Liu, H. Lee, Y. Xiong, C. Sun, X. Zhang, *Science* **315**, 1686 (2007).
10. M. Nakahara, *Geometry, Topology and Physics* (IOP Publishing, Bristol, UK, ed. 2, 2003).
11. M. Monastryskiy, *Riemann Topology and Physics* (Birkhäuser, Boston, ed.2, 1999).
12. I. M. Lifshitz, *Sov. Phys. JETP* **11**, 1130 (1960).
13. A. M. Kosevich, *Low Temp. Phys.* **30**, 97 (2004).
14. M. Born, E. Wolf, *Principles of Optics* (Cambridge Univ. Press, Cambridge, ed. 7, 2002).
15. P. Yao *et al.*, *Phys. Rev. B* **80**, 195106 (2009).
16. Z. Jacob, I. Smolyaninov, E. Narimanov, arXiv:0910.3981v2 [physics.optics] (2009).
17. M. A. Noginov *et al.*, *Opt. Lett.* **35**, 1863 (2010).
18. Z. Jacob *et al.*, *Appl. Phys. B* **100**, 215 (2010).
19. A. N. Poddubny, P. A. Belov, Y. S. Kivshar, *Phys. Rev. A* **84**, 023807 (2011).
20. O. Kidwai, S. V. Zhukovsky, J. E. Sipe, *Opt. Lett.* **36**, 2530 (2011).
21. A complete description of the fabrication, characterization, and modeling is available as supplementary materials on *Science* Online.
22. A. J. Hoffman *et al.*, *Nat. Mater.* **6**, 946 (2007).
23. G. W. Ford, W. H. Weber, *Phys. Rep.* **113**, 195 (1984).
24. M. D. Leistikow, J. Johansen, A. J. Kettelarij, P. Lodahl, W. L. Vos, *Phys. Rev. B* **79**, 045301 (2009).
25. M. L. Andersen, S. Stobbe, A. S. Sørensen, P. Lodahl, *Nat. Phys.* **7**, 215 (2011).
26. K. Okamoto, S. Vyawahare, A. Scherer, *J. Opt. Soc. Am. B* **23**, 1674 (2006).
27. I. Contijo *et al.*, *Phys. Rev. B* **60**, 11564 (1999).
28. L. B. Felsen, N. Marcuvitz, *Radiation and Scattering of Waves* (IEEE, New York, 1994).

Acknowledgments: V.M.M. and H.N.S.K. acknowledge partial support through the Materials Research Science and Engineering Center program of the National Science Foundation through grant DMR 1120923 and the Army Research Office (ARO) grant W911NF0710397. V.M.M. and I.K. acknowledge support through Round 14 of the CUNY Collaborative Incentive Research Grant Program. E.N. was partially supported by ARO–Multidisciplinary University Research Initiative grants 50342-PH-MUR and W911NF-09-1-0539. Z.J. was partially

supported by Natural Sciences and Engineering Research Council of CanadaDiscovery grant 402792 and Canadian School of Energy and Environment Proof of Principle Grant. The ellipsometric measurements were carried out at the Center for Functional Nanomaterials at Brookhaven National Laboratory, which is supported by the U.S. Department of Energy, Office of Basic Energy Sciences, under contract DE-AC02-98CH10886.

Supplementary Materials
www.sciencemag.org/cgi/content/full/336/6078/205/DC1
Materials and Methods
Figs. S1 to S6
References (*29*, *30*)

16 January 2012; accepted 7 March 2012
10.1126/science.1219171

Ferroelectric Columnar Liquid Crystal Featuring Confined Polar Groups Within Core–Shell Architecture

Daigo Miyajima,[1] Fumito Araoka,[2] Hideo Takezoe,[2]* Jungeun Kim,[3] Kenichi Kato,[4] Masaki Takata,[3,4] Takuzo Aida[1]*

Ferroelectric liquid crystals are materials that have a remnant and electrically invertible polar order. Columnar liquid crystals with a ferroelectric nature have potential use in ultrahigh-density memory devices, if electrical polarization occurs along the columnar axis. However, columnar liquid crystals having an axial nonzero polarization at zero electric field and its electrical invertibility have not been demonstrated. Here, we report a ferroelectric response for a columnar liquid crystal adopting a core–shell architecture that accommodates an array of polar cyano groups confined by a hydrogen-bonded amide network with an optimal strength. Under an applied electric field, both columns and core cyano groups align unidirectionally, thereby developing an extremely large macroscopic remnant polarization.

Ferroelectric liquid crystals (FLCs) have potential application in lightweight, easy-processable electrical devices for fast-switching displays, rewritable memories, and nonlinear optics (*1*). For liquid crystalline (LC) materials to operate ferroelectrically, a nonzero polarization at zero electric field (E-field), together with its electrical invertibility, is a prerequisite. However, this goal is difficult to realize, particularly in dynamic molecular systems such as LC materials, as once oriented electrically, polar motifs reorganize spontaneously at zero E-field in such a way that their dipoles cancel each other either macroscopically or locally. Although FLCs with a smectic geometry (Fig. 1, A and B) have been reported (*2*–*5*), most require cell

[1]Department of Chemistry and Biotechnology, School of Engineering, The University of Tokyo, 7-3-1 Hongo, Bunkyo-ku, Tokyo 113-8656, Japan. [2]Department of Organic and Polymeric Materials, Tokyo Institute of Technology, 2-12-1 O-okayama, Meguro-ku, Tokyo 152-8552, Japan. [3]Japan Synchrotron Radiation Research Institute (JASRI), 1-1-1 Kouto, Sayo-cho, Sayo-gun, Hyogo 679-5148, Japan. [4]RIKEN SPring-8 Center, 1-1-1 Kouto, Sayo-cho, Sayo-gun, Hyogo 679-5148, Japan.

*To whom correspondence should be addressed. E-mail: takezoe.h.aa@m.titech.ac.jp (H.T.); aida@macro.t.u-tokyo.ac.jp (T.A.)

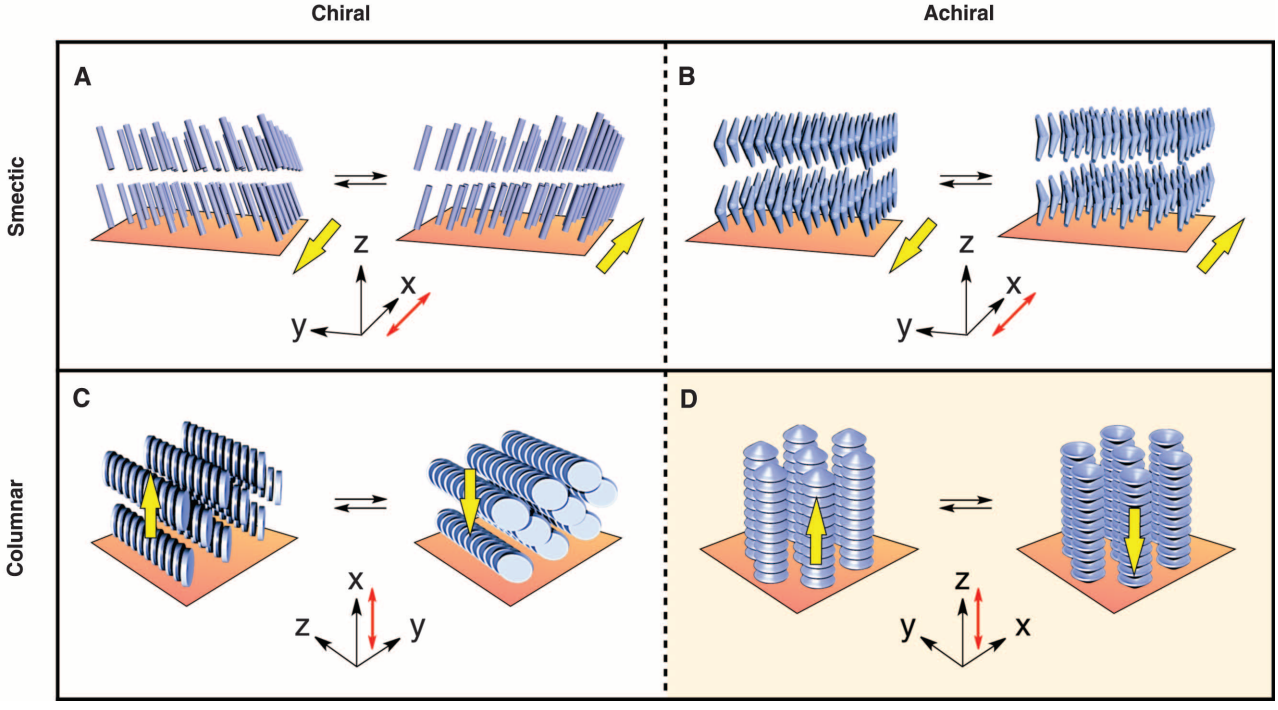

Fig. 1. Schematic illustrations of the electrical polarization behaviors of ferroelectric liquid crystals (FLCs) with four different geometries. (**A**) and (**B**) illustrate the behaviors of smectic-type FLCs consisting of chiral rod-shaped and achiral bent-shaped molecules, respectively, whereas (**C**) and (**D**) represent those of columnar FLCs composed of chiral discotic and achiral umbrella-shaped molecules, respectively. Red and yellow arrows denote the directions of an applied electric field (E-field) and the resulting polarization, respectively. Chiral rod-shaped molecules generate a layer polarization in the *x*-*y* plane. However, no macroscopic polarization develops because such a layer polarization is canceled owing to its helical orientation with the helical axis along the *z* direction. To develop a macroscopic polarization, a thin cell has been used so that an enhanced cell-surface effect unwinds the helical geometry as shown in (A). Achiral bent-shaped molecules, which likewise generate a layer polarization in the *x*-*y* plane, do not assemble in a helical geometry, so that a macroscopic polarization develops as shown in (B). Columnarly assembled chiral discotic molecules adopt a helical geometry, which generates a polarization in a perpendicular direction (*x* direction) to the columnar axis when the helical geometry is unwound by means of a cell-surface effect as shown in (C). In contrast to (A) to (C), columnarly assembled achiral umbrella-shaped molecules (this work) generate a polarization along the columnar axis (*z* direction). Therefore, unidirectional orientation of such columns results in the development of a macroscopic polarization as shown in (D).